International Journal of Pressure Vessels and Piping 86 (2009) 164–176

Contents lists available at ScienceDirect

International Journal of Pressure Vessels and Piping

journal homepage: www.elsevier.com/locate/ijpvp

Failure assessments of corroded pipelines with axial defects using stress-based criteria: Numerical studies and verification analyses

Mario S.G. Chiodo, Claudio Ruggieri*

Department of Naval Architecture and Ocean Engineering, University of São Paulo, Av. Prof. Mello Moraes, 2231 (PNV-EPUSP), São Paulo, SP 05508-030, Brazil

ARTICLE INFO

Article history:
Received 15 April 2008
Received in revised form
21 August 2008
Accepted 10 November 2008

Keywords:
Corrosion defects
Pipelines
Defect assessment
Failure assessment
Limit load
Burst testing

ABSTRACT

Conventional procedures used to assess the integrity of corroded piping systems with axial defects generally employ simplified failure criteria based upon a plastic collapse failure mechanism incorporating the tensile properties of the pipe material. These methods establish acceptance criteria for defects based on limited experimental data for low strength structural steels which do not necessarily address specific requirements for the high grade steels currently used. For these cases, failure assessments may be overly conservative or provide significant scatter in their predictions, which lead to unnecessary repair or replacement of in-service pipelines. Motivated by these observations, this study examines the applicability of a stress-based criterion based upon plastic instability analysis to predict the failure pressure of corroded pipelines with axial defects. A central focus is to gain additional insight into effects of defect geometry and material properties on the attainment of a local limit load to support the development of stress-based burst strength criteria. The work provides an extensive body of results which lend further support to adopt failure criteria for corroded pipelines based upon ligament instability analyses. A verification study conducted on burst testing of large-diameter pipe specimens with different defect length shows the effectiveness of a stress-based criterion using local ligament instability in burst pressure predictions, even though the adopted burst criterion exhibits a potential dependence on defect geometry and possibly on material's strain hardening capacity. Overall, the results presented here suggests that use of stress-based criteria based upon plastic instability analysis of the defect ligament is a valid engineering tool for integrity assessments of pipelines with axial corroded defects.

1. Introduction

Accurate predictions of the residual strength for corroded piping systems remain essential in fitness-for-service analyses of oil and gas transmission pipelines, including onshore and offshore facilities. As the pipeline infrastructure ages, metal loss due to corrosion represents a major source of material degradation in steel pipes which most often reduces its burst strength with increased potential for catastrophic failure [1]. High resolution techniques are now available which provide accurate measurements of the corrosion defect geometry. However, the increased accuracy of defect measurement techniques may be insufficient to guarantee high levels of reliability in burst pressure predictions of corroded pipelines due to the rather empirical nature of conventional integrity assessment procedures. Current codes and standards for defect assessments of corroded oil and gas pipelines, such as ASME B31.G [2], RSTRENG [3], DNV RP-F101 [4] among others, provide simplified acceptance criteria which are derived based upon a limit-load solution for a blunted axial crack-like flaw in a pressurized vessel or pipe. While these widely used acceptance criteria for linepipe defects clearly simplify integrity assessments of in-service piping components, they essentially reflect a semi-empirical analysis calibrated by extensive burst testing of relatively thin-walled pipes containing machined cracks conducted on low-to-moderate strength structural steels (API Grades X52 and X60) [5–8].

It became apparent over recent years that conventional defect assessment procedures for corroded pipelines have limited ability to predict the failure of damaged piping systems in a realistic manner. Most often, these procedures provide unduly conservative and overly pessimistic predictions. While such conservatism represents an extra factor of safety, excessive pessimism in corrosion defect assessments can lead to unwarranted repairs or replacement of in-service pipelines at great operational costs. Moreover, the failure equations incorporated into current codes for defect assessments of corroded pipelines do not necessarily address specific requirements for the higher grade steels currently used. Indeed, high strength steels (such as API X100 and X120) applicable for high pressure pipelines exhibit much lower strain hardening capacity and lower strain to failure when compared to low-to-moderate strength

* Corresponding author. Tel.: +55 11 30915350; fax: +55 11 30915717.
E-mail address: claudio.ruggieri@poli.usp.br (C. Ruggieri).

0308-0161/$ – see front matter © 2008 Elsevier Ltd. All rights reserved.
doi:10.1016/j.ijpvp.2008.11.011

pipeline steels. Such features may have a strong impact on failure predictions of damaged pipelines made of higher grade materials based upon conventional failure assessment procedures. Recent exploratory studies [9] suggest that an X100 steel is likely to be less damage tolerant than a lower grade material such as an X60 steel.

The above observations prompted further developments in conventional methodologies to assess the significance of corrosion defects. These procedures have evolved primarily along the use of approaches based upon stress-based criteria [10–14]. Here, failure occurs when the equivalent stress (such as the von Mises stress) over the remaining defect ligament reaches a reference stress, σ_{ref}, which is defined as a fraction of the true ultimate tensile stress, $\overline{\sigma}_{\text{u}}$, i.e., $\sigma_{\text{ref}} = \eta\overline{\sigma}_{\text{u}}$, where η often ranges from 0.8 to 1.0. These research efforts have been relatively effective in producing more accurate failure predictions of corroded pipes removed from service. However, while these studies report agreement between predictions and actual failure pressure within $\pm 10\%$ deviation, the η-factor adopted to specify the reference stress criterion appears to depend upon defect configuration and material properties. Indeed, the analyses conducted by Choi et al. [13] suggest that $\eta = 0.9$ for rectangular-shaped defects whereas $\eta = 0.8$ for elliptical defects. Failure criteria for use in defect assessments should provide integrity analyses which are reasonably invariant to such factors. Consequently, development of robust methods for structural integrity analyses become central to specifying critical defect sizes which enter directly into procedures for repair decisions and life-extension programs of in-service piping components. Perhaps more importantly, these procedures must ensure fail-safe operations which avoid costly leaks and ruptures due to material failure to comply with the current stringent environment-based regulations.

This study examines the applicability of a stress-based criterion based upon plastic instability analysis to predict the failure pressure of corroded pipelines with axial defects. A central focus is to gain additional insight into effects of defect geometry and material properties on the attainment of a local limit load to support the use of stress-based burst strength criteria. The presentation begins with a description of the fracture mechanics analysis for a planar flaw which forms the basis of current defect acceptance criteria for corroded pipelines. This is followed by a parametric study conducted on plane-strain models for a flawed pipe containing an axial defect with varying geometry and material flow properties. These analyses provide an extensive body of results which lend further support to adopt failure criteria for corroded pipelines based upon ligament instability analyses. Verification analyses conducted on burst testing of large-diameter pipe specimens with varying defect configuration made of API X65 and X100 steels show the effectiveness of a stress-based criterion using $\overline{\sigma}_{\text{ref}} = \eta\overline{\sigma}_{\text{u}}$ in burst pressure predictions, even though the η-factor exhibits a potential dependence on defect geometry and possibly on material's strain hardening capacity. Overall, the results presented here suggests that use of stress-based criteria based upon plastic instability analysis of the defect ligament is a valid engineering tool for integrity assessments of pipelines with axial corroded defects.

2. Overview of defect acceptance criteria for corroded pipelines

Experimental studies and *in situ* observations consistently reveal that plastic collapse is the dominant failure mode for thin-walled pressurized pipes with crack-like flaws including corrosion defects. In this regime, cracked or flawed pipes and cylindrical vessels made of a hardening material, such as pipeline grade structural steels, can withstand large increases in pressure loading following the beginning of yielding without substantial loss of its load bearing capacity. Conventional methodologies to define acceptance criteria for axially-oriented corrosion defects in gas and oil transmission pipelines have evolved primarily along two lines of development: approaches based upon a failure stress criteria derived from a fracture mechanics analysis of a planar (crack-like) flaw, and approaches based upon a plastic collapse analysis of a cracked flaw. For ductile materials, however, both approaches reflect essentially a limit load solution for a thin-walled pipes and cylindrical vessels under internal pressure with an axial crack (including a surface crack or a through-thickness defect) so they lead to similar burst strength predictions.

Standard limit load analysis conventionally defines the global limit load (also referred to as net-section limit load) at which displacements become unbounded or unrestricted [16] thereby increasing very rapidly with little or no increase in the corresponding applied loading. Once displacements reach this point, the structure attains its maximum load-bearing capacity. When a surface crack-like flaw or a surface corrosion defect is present in the structure, the picture becomes more complex as the limit load can now be defined in terms of local instability of the remaining ligament ahead of crack or defect. While a number of limit load solutions for cracked pipes and cylindrical vessels are available in the literature (see, e.g., [17–20]) including finite element solutions (see Ref. [13] for representative solutions), there is still a certain degree of ambiguity in defining the limit load, particularly in the case of corroded pipelines.

The development of plasticity in a cracked (defective) pipe depends primarily on the crack (defect) configuration, pipe geometry, loading type (internal pressure, bending, axial tension or a combination of these loads) and boundary conditions (plane stress, plane strain, multiaxial stress state). Limiting attention to an axially-oriented defect in a pipe under internal pressure, the failure pressure, P_{f}, can be related to key geometric parameters in nondimensional form given by

$$\frac{P_{\text{f}}}{P_0} = \mathcal{L}\left(\frac{a}{t}; \frac{a}{c}; \frac{t}{D}; \cdots\right) \tag{1}$$

where $\mathcal{L}$ is a function of crack or defect geometry. In the above expression, D is the pipe outside diameter, t is the pipe wall thickness, a denotes the defect depth, c represents the half-length of the defect (see Fig. 1) and P_0 defines a "baseline" failure pressure solution for a defect-free pipe (see Eq. (11) for a representative burst pressure for a defect-free pipe). Numerous limit load solutions (including global and local limit loads) for these configurations are available which consider essentially pipe and defect geometry as well as loading type. A comprehensive set of such solutions is provided in Miller [17] and SINTAP [19]; in particular, the limit load solutions available in the SINTAP procedure derive from previous work of Carter [21] based upon lower bound theorems. In a series of recent articles, Staat [22–24] discuss some points of criticism on the limit load solutions of Miller [17] and Carter [21] and provide some improved formulations which are most applicable to thick pipes and cylindrical vessels.

However, for surface external defects in thin-walled pipes, such as most typical corrosion defects in oil and transmission pipelines, a consensus has developed for the use of the early work by Kiefner et al. [5] to address the burst strength of axially-oriented flaws in pressurized pipes by means of the connection between the stress level at the remaining ligament of the flaw and pipe failure (burst). Their approach builds upon the strip-yield model [28] shown in Fig. 1(a) to define the crack tip opening displacement (CTOD or δ) for a through crack in a infinite plate subjected to a remote tensile stress, σ, in the form

$$\delta = \frac{8\sigma_{\text{ys}}c}{\pi E} \ln \sec\left(\frac{\pi}{2}\frac{\sigma}{\sigma_{\text{ys}}}\right) \tag{2}$$

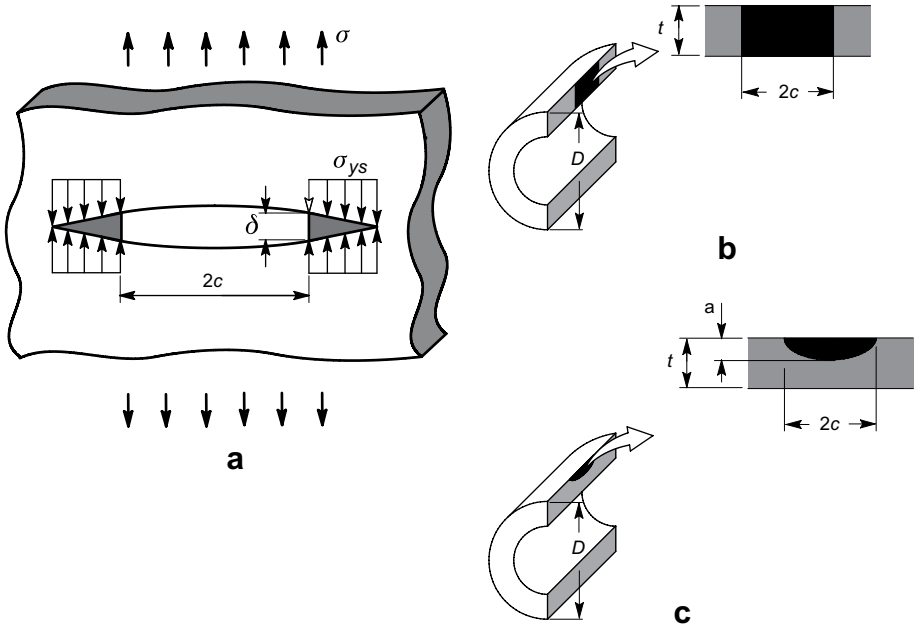

Fig. 1. Strip yield model and crack geometry employed to derive a failure criteria for axially corroded pipelines based upon a fracture mechanics analysis of a planar defect.

where σ_{ys} is the material's yield stress, E is the (longitudinal) elastic modulus and $2c$ denotes the total axial crack length. Here, it is understood that the above expression holds true for plane stress conditions and a nonhardening material (see Ref. [28] for further details on the strip-yield model).

Consider now the thin-walled pipe under pressure loading with an axially oriented, through-thickness crack illustrated in Fig. 1(b). For this crack configuration, the strip-yield model given by Eq. (2) can be rewritten as

$$\delta = \frac{8\sigma_{ys}c}{\pi E}\ln\sec\left(\frac{\pi}{2}\frac{M_T\sigma_h}{\sigma_{ys}}\right) \tag{3}$$

where σ_h is the hoop (membrane) stress acting on the crack face. Factor M_T introduced by Folias [29,30] represents a nondimensional parameter which accounts for the stress amplification at the ends of axially-oriented defects in curved shells (such as a pipe) caused by the outward deflection (most often termed "bulging" of the pipe). The Folias bulging factor defines the relationship between the crack driving forces for a cracked pipe (or cylindrical vessel) and a cracked flat plate with same crack size such that

$$M_T = K_{Shell}/K_{Plate} \tag{4}$$

where K_{Shell} and K_{Plate} are the elastic stress intensity factors for the cracked curved shell (pipe) and cracked flat plate.

A number of expressions for the M_T-factor have been proposed with varying levels of conservatism and accuracy associated with the relative crack length as defined by the shell parameter $\lambda = c/\sqrt{Rt}$, where R is the outside pipe radius ($R = D/2$ – see Fig. 1). A widely used expression takes the form [29,30]

$$M_T = \sqrt{1+\beta\lambda^2} \tag{5}$$

where several values for the constant β are possible. For instance, ASME B31.G [2] adopts $\beta = 1.61$ for short defects ($\lambda < 3.2$) which yields conservative M_T-factors whereas DNV F-101 [4] utilizes $\beta = 0.62$ (with no restriction made on defect length) and RSTRENG [3] adopts $\beta \approx 1.25$ for $\lambda < 5.0$ (here, the original square term in Ref. [3] is neglected for comparison purposes since its contribution to the corresponding M_T-factor is small).

To arrive at an approximate failure criterion for a pressurized pipe with a through-thickness axial flaw, the development outlined above proceeds as follows. By assuming a fully ductile material and making $\delta \to \infty$ in the previous strip-yield model, Kiefner et al. [5] proposed a simpler form of Eq. (3) given by

$$M_T\sigma_h = \sigma_{ref} \tag{6}$$

with the material's yield stress, σ_{ys}, replaced by a reference stress, σ_{ref}, which is most often adopted as the (engineering) ultimate tensile stress, σ_u, or the flow stress, $\sigma_f = (\sigma_u + \sigma_{ys})/2$. Moreover, in the limit when the defect length $2c \to 0$, parameter $M_T \to 1$ so that Eq. (6) reduces to the standard failure criterion for an uncracked pipe.

To provide a simpler extension of the failure stress criterion applicable to a pressurized pipe with a surface crack (see Fig. 1(c)), the bulging factor M_T appearing in Eq. (6) is replaced by factor M_S which is defined by Kiefner et al. [5] as

$$M_S = \frac{1 - a/(M_T t)}{1 - a/t} \tag{7}$$

thereby yielding

$$M_S\sigma_h = \sigma_{ref}. \tag{8}$$

The failure stress criterion for a pressurized pipe with a surface flaw given by the above expression has been validated by extensive full scale testing of cracked pipes with varying crack configurations and material properties. While it possesses a semi-empirical character, Eq. (8) forms the basis of established defect assessment procedures for corroded oil and gas pipelines, including ASME B31.G [2], RSTRENG [3], DNV F–101 [4], API 579 [20] among others.

In the above failure stress criteria for through-thickness and surface crack-like defects, factor M_T influences the levels of the hoop stress acting on the remaining ligament thereby potentially affecting burst strength predictions. Fig. 2(a) displays the variation of σ_h/σ_{ref} with increased shell parameter, λ, for a through-thickness defect and three widely different β-values. Fig. 2(b) shows the dependence of σ_h/σ_{ref} on defect depth as measured by the a/t-ratio with increased shell parameter, λ, for a surface defect with a fixed

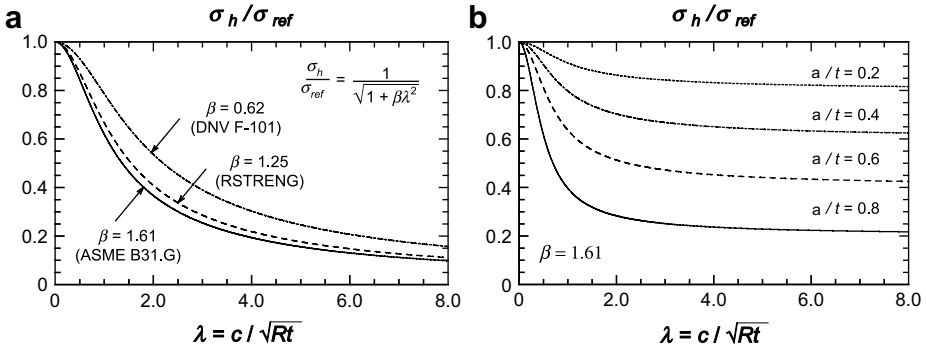

Fig. 2. (a) Variation of factor M_T with increased shell parameter for a through-thickness defect; (b) Dependence of factor M_S on defect depth with increased shell parameter for a surface defect.

value for the shell parameter $\beta = 1.61$. In both plots, the shell parameter covers a relatively wide range of short ($\lambda \lesssim 4.0$) and long defects ($\lambda \gtrsim 6.0$).

Consider first the results displayed in Fig. 2(a). While the β-value sets the severity of stress amplification on the remaining ligament due to pipe bulging, there is only a moderate effect on the σ_h/σ_{ref}-ratio, particularly for long defects ($\lambda \gtrsim 6.0$). For shorter cracks ($\lambda \lesssim 4.0$), the dependence of the σ_h/σ_{ref}-ratio on β is a little more pronounced. For example, at $\lambda = 2.0$ the stress ratio, σ_h/σ_{ref}, changes from ~0.35 for $\beta = 1.61$ to ~0.55 for $\beta = 0.62$. However, it should be emphasized that such behavior does not necessarily translate into a weak effect of parameter β on the burst strength since, for example, doubling the β-value would imply a reduction of circa 30% in the σ_h/σ_{ref}-ratio. Indeed, as it will be discussed in Section 4, as the failure pressure for the pipe is approached (thereby marking the plastic local instability of the remaining ligament), small increases in the pressure loading causes rapid spread of the damaged area in the remaining ligament with strong impact on the burst strength.

Consider next the results displayed in Fig. 2(b). For a fixed value of $\beta = 1.61$, the stress ratio σ_h/σ_{ref} varies strongly, particularly for deep flaws, in the short crack range ($\lambda \leq 2.0$). After this transient region, the σ_h/σ_{ref}-ratio is relatively insensitive to flaw length for all a/t-ratios. The weak dependence of σ_h/σ_{ref}-ratios on flaw length for $\lambda > 2.0$ derives from the observation that stress fields in the remaining ligament vary primarily due to flaw depth for longer flaws. Similar trends are also obtained for other β-values. These results clearly show that the growth of short and deep flaws (which might be undetected during routine inspection) across the pipe wall thickness due to fatigue or further corrosion mechanisms may have a strong adverse impact on the structural integrity of the pipe or vessel. Moreover, for very short ($\lambda \lesssim 3.0$) and deep ($a/t \gtrsim 0.8$) defects, the failure stress for a through-thickness flaw is higher than the corresponding failure stress for a surface flaw. While not addressed in the present context, such behavior may be associated with a leak-before-break condition [18] in which the ligament failure for the surface flaw creates a stable through-thickness defect.

While the previous approaches have been effective in integrity assessments of corroded pipelines and form the basis for industrial codes and guidelines for fitness-for-service analyses of local thinned areas of piping components, the semiempirical nature of Eq. (8) has raised some points of criticism. In particular, the industry experience suggests that defect assessment procedures based upon Eq. (8) may be overly conservative depending upon pipeline steel grade and corrosion defect geometry. The analyses described subsequently employ a failure stress criterion based upon plastic instability of the defect ligament to produce less conservative burst strength predictions.

3. Finite element procedures

3.1. Parametric studies of flawed pipes

Nonlinear finite element analyses are described for plane-strain models of axially flawed pipes with $D = 508$ mm (20 in.), $t = 15$ mm ($D/t = 34$) and external surface defects having $a/t = 0.2$ (shallow defect) and $a/t = 0.5$ (deep defect). Here, a is the crack depth, t is the pipe wall thickness and D is the pipe outside diameter. These configurations typify common geometries and flaw sizes in high pressure, high strength pipelines. To verify the effect of flaw shape and flaw width on corrosion defect assessments incorporating stress-based criteria, the matrix analysis considers groove-shaped defects with groove width, $d_g = 0.2$, 0.5, 1, 3 and 6 mm, and rectangular-shaped defects with defect width, $w_c = 25$, 50, 75, 100 and 200 mm. Fig. 3 illustrates the flaw geometry adopted in the analyses.

Fig. 4(a-c) shows the finite element models constructed for the pipe configurations having $a/t = 0.2$ with $d_g = 1$ mm (groove shape) and $w_c = 25$ mm (rectangular shape). Symmetry conditions permit modeling of only one-half of the analyzed pipes. Square elements of uniform size are defined in the defect region and along the remaining ligament to provide similar levels of mesh refinement for all numerical models. Because no strong stress gradients arise in the defect region (which contrasts to conventional crack-tip problems – see, for example, Ruggieri and co-workers [25,26] for illustrative analyses), the evolving stresses ahead of ligament with increased pressure are resolved adequately for element sizes of $\approx 0.1 \sim 0.5$ mm. The half-symmetric model has one thickness layer of 1770 8-node, 3-D elements (3970 nodes) with plane-strain constraints ($w = 0$) imposed on each node. Very similar finite element models and mesh details are employed for other pipe configurations.

3.2. 3-D burst analysis of API X65 corroded pipes

Finite element analyses are also conducted for numerical models of corroded pipes with outside diameter, $D = 762$ mm (30 in.) and wall thickness, $t = 17.5$ mm ($D/t = 44$). Kim et al. [14] performed burst tests on end-capped pipe specimens made of API 5L X65 with length, $L = 2.3$ m. Rectangular-shaped corrosion defects with varying geometry were machined on the outside surface of the pipes. The analysis matrix includes corrosion defects with fixed depth, $a = 8.75$ mm ($a/t = 0.5$), circumferential extent (width), $w_c = 50$ mm and varying corrosion length, $2c = 50$, 100, 200, 300, 600 and 900 mm (see Fig. 3).

Fig. 5 shows the finite element model for the 3-D analysis of the pipe specimen with $2c = 900$ mm. Very similar numerical models and mesh details are employed for other pipe configurations. Symmetry conditions permit modeling of only one-quarter of the

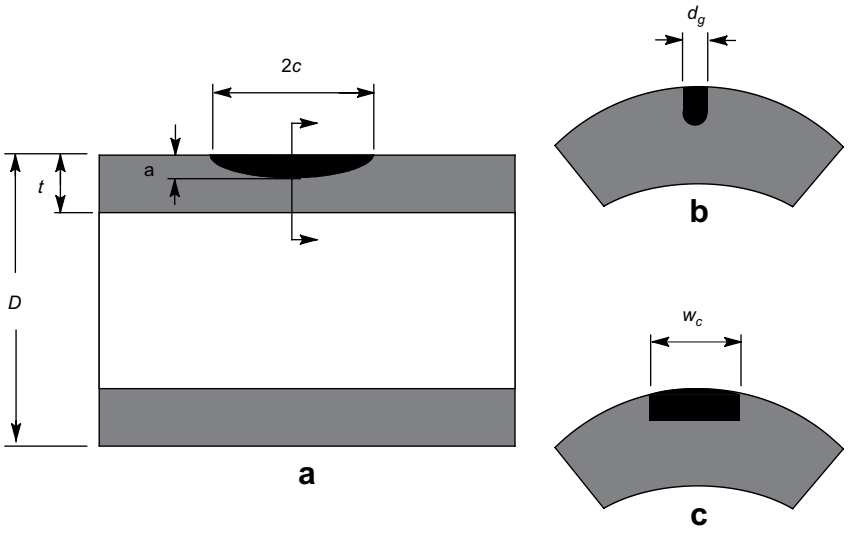

Fig. 3. Pipe configuration and defect geometry employed in the analyses.

specimen with appropriate constraints imposed on the symmetry planes. The quarter-symmetric model has ≈90,000 8-node, 3-D elements arranged into several variable thickness layers over the half-length ($L/2$), as illustrated in Fig. 5(a), to accommodate the potential stress gradients in the defect region, particularly at the corner edges. While the machined corrosion defects have rounded corner edges with a 5 mm radius [14], the analyzed 3-D models have square corner edges to facilitate mesh construction. As noted previously, because no strong stress gradients arise in the defect region, the evolving stresses ahead of ligament with increased pressure are not affected by this mesh detail. Indeed, numerical analyses employed to assess the adequacy of mesh refinement reveal that predictions of failure pressure with and without the round corner edge are essentially similar. To simulate the end-capped condition of the burst tests, the pipe specimens were loaded under increasing internal pressure coupled with axial stresses imposed at the pipe ends.

3.3. 3-D burst analysis of API X100 pipes with axial flaws

Mannucci et al. [15] recently reported on full-scale burst tests at room temperature conducted on large diameter pipes with axial surface defects made of a high strength, API 5L X100 grade steel. The burst tests include end-capped pipe specimens with two outside diameters: (1) $D = 914$ mm (36 in.) and wall thickness, $t = 16$ mm ($D/t = 57$) with $2c = 150 \times a = 9$ mm and $2c = 450 \times a = 6$ mm; (2) $D = 1422$ mm (56 in.) and wall thickness, $t = 19.1$ mm ($D/t = 74$) with $2c = 180 \times a = 10.4$ mm (refer to Fig. 3).

Fig. 6 shows the finite element model for the 3-D analysis of the pipe specimen with $D = 914$ mm (36 in.) and $2c = 150 \times a = 9$ mm. The general mesh construction follows closely the previous finite

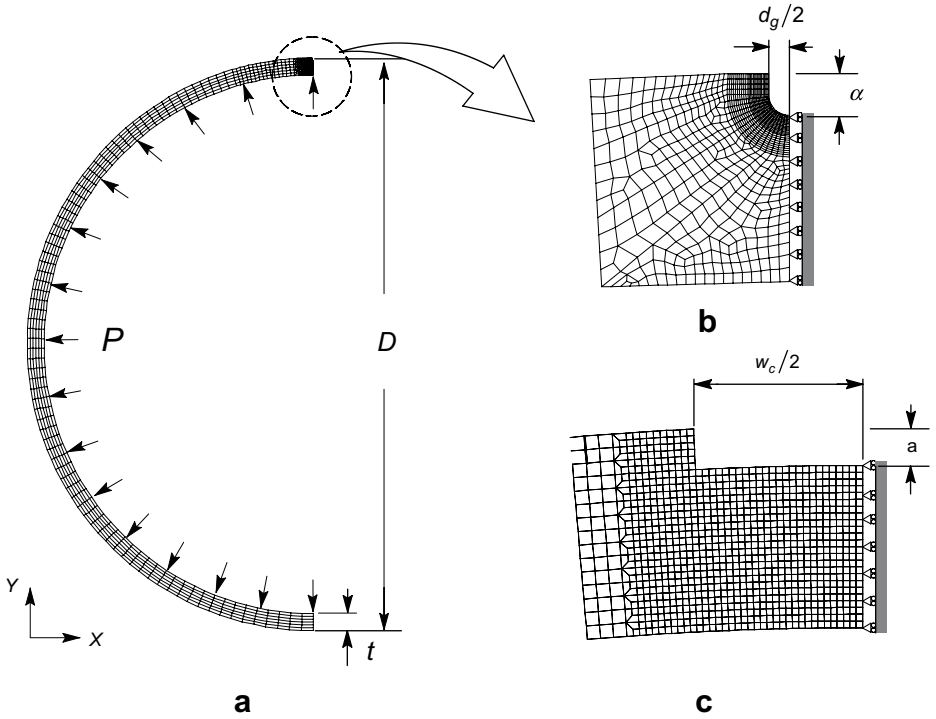

Fig. 4. (a) Plane-strain finite element model for the analyzed pipe with a/t=0.2; (b) Mesh detail for the groove-shaped defect; (c) Mesh detail for the rectangular-shaped defect.

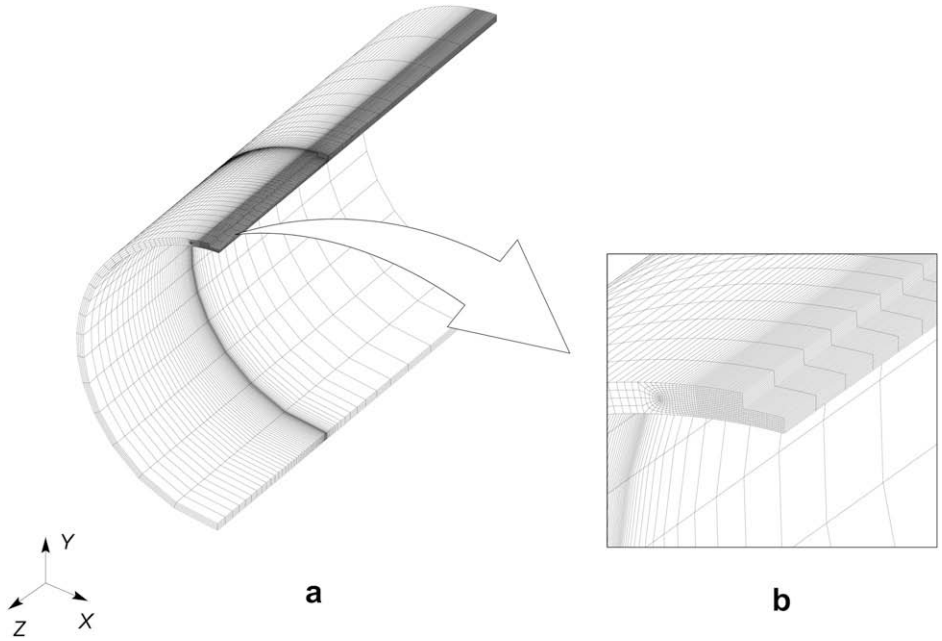

Fig. 5. 3-D finite element model for the X65 pipe specimen with $2c = 900$ mm defect tested byKim et al. [14].

element models for the X65 pipes. The quarter-symmetric model has ≈26,000 8-node, 3-D elements arranged into several variable thickness layers over the pipe half-length, as illustrated in Fig. 6(a). A groove-shaped flaw with groove width $d_g = 0.5$ mm is employed to model the axial surface defect for the pipe specimens as depicted in Fig. 6(b). As it will be discussed in Section 4, the groove width does not affect predictions of burst pressure based upon the approach adopted in the present work.

3.4. Material models and solution procedures

The elastic-plastic material employed in the parametric analyses described in Section 4 follows a J_2 flow theory with conventional Mises plasticity in small geometry change (SGC) setting. The uniaxial true stress ($\overline{\sigma}$) *vs.* logarithmic strain ($\overline{\epsilon}$) curve obeys a simple power-hardening model

$$\frac{\overline{\epsilon}}{\epsilon_{ys}} = \frac{\sigma}{\sigma_{ys}} \quad \overline{\epsilon} \le \epsilon_{ys}; \quad \frac{\overline{\epsilon}}{\epsilon_{ys}} = \left(\frac{\overline{\sigma}}{\sigma_{ys}}\right)^n \overline{\epsilon} > \epsilon_{ys} \tag{9}$$

where σ_{ys} and ϵ_{ys} are the yield stress and strain, and $n$is the strain hardening exponent. These finite element analyses consider material flow properties covering most pipeline and pressure vessel steels: $n = 5$ $(E/\sigma_{ys} = 800)$, 10 $(E/\sigma_{ys} = 500)$ and 20 $(E/\sigma_{ys} = 300)$ with $E = 206$ GPa and $\nu = 0.3$; these ranges of properties also reflect the upward trend in yield stress with the increase in strain hardening exponent, n, characteristic of ferritic steels. The stress–strain response for these materials is shown in Fig. 7(a).

Evaluation of plastic instability in the remaining defect ligament through the stress-based criterion employed in Sections 4 and 5 requires specification of the true tensile stress, $\overline{\sigma}_u$. For each material property set adopted in the parametric analyses, $\overline{\sigma}_u$ is estimated using the following relationship [28]:

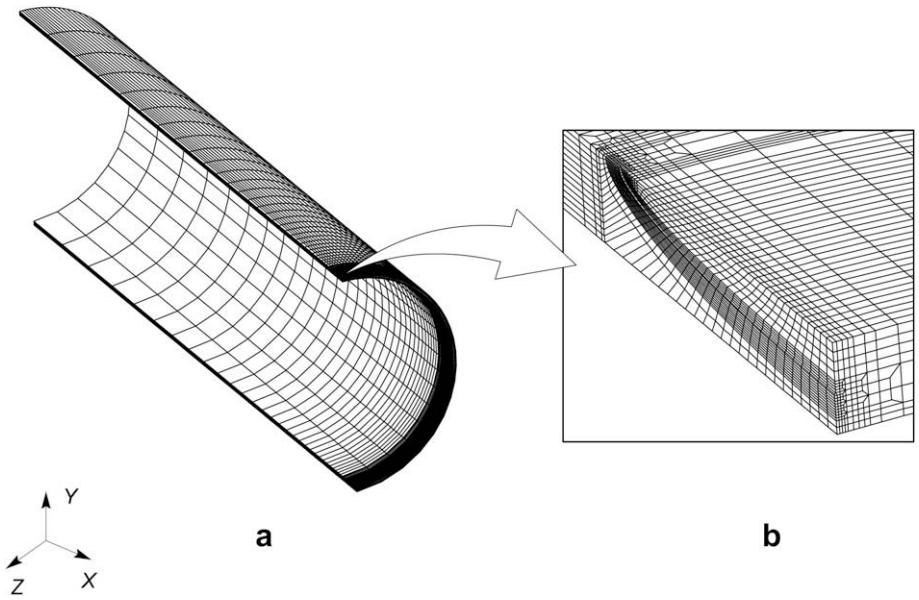

Fig. 6. 3-D finite element model for the X100 pipe specimen with $D = 914$ mm (36 in.) and $2c = 150 \times a = 9$ mm defect tested by Mannucci et al. [15].

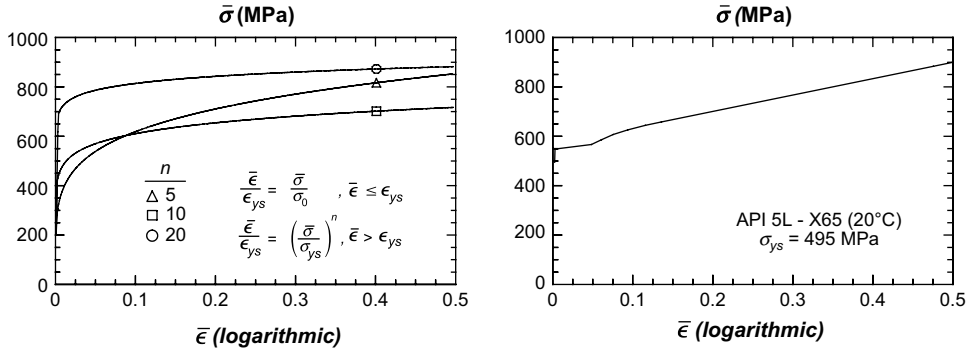

Fig. 7. (a) Uniaxial true stress-logarithmic strain response of materials employed in the parametric analyses using a power-hardening model; (b) Uniaxial true stress-logarithmic strain response for the tested API X65 [14].

$$\bar{\sigma}_u = \sigma_{ys}\left[\frac{(500N)^N}{\exp(N)}\right] \tag{10}$$

where $N = 1/n$.

Section 5 describes numerical analyses for pipe specimens that were tested by Kim et al. [14] and Mannucci et al. [15]. The true stress-logarithmic strain behavior for the X65 pipeline steel of the specimens tested by Kim et al. [14] is modeled with a piecewise linear approximation to the measured tensile response as shown in Fig. 7(b). For the X100 pipeline steel, we adopt the tensile properties provided by Mannucci et al. [15] to approximate the true stress-logarithmic strain response by the power-hardening law given by Eq. (9) with the strain hardening exponent derived from previous Eq. (10). All these analyses also consider Young's modulus $E = 206$ GPa and Poisson's ratio $\nu = 0.3$.

The numerical computations reported here are generated using the research code WARP3D [31] which implements a very efficient, sparse matrix solver that significantly reduces both memory and CPU time required for solution of the linearized equations compared to conventional direct solvers. A typical analysis of the 3-D pipe models to reach ligament instability requires approximately 300 load steps solved in less than 10 h in an SGI Itanium-based workstation.

4. Plastic instability analyses for pipes with axial defects

The following sections provide key results of the extensive plane-strain analyses conducted on pipes with axial flaws. Primary attention is given to the development of plasticity in the remaining ligament ahead of defect coupled with the evolving levels of stress fields with increased pressure loading. The presentation considers plane-strain analyses of the pipe specimens with a groove-shaped flaw and a rectangular-shaped defect which encompasses a wide range of defect geometry and different material properties as defined by the yield stress and hardening behavior. Although a number of previous analyses and theoretical arguments show that conventional limit load solutions are fairly insensitive to mesh details, systematic studies that address effects of defect geometry and defect size on the failure pressure for varying hardening materials remain relatively rare. Consequently, analyses exploring the influence of defect shape effects (groove *vs.* rectangular) on the evolution of the highly stressed zones in the remaining defect ligament prove useful to further verify the applicability of burst strength criteria based upon the attainment of a local limit load.

4.1. Fully plastic behavior under internal pressure

The extensive finite element analyses of pipe configurations including the effects of defect shape provide additional support to define the limit load in terms of local instability of the remaining ligament ahead of defect. Figs. 8–11 display the growth of Mises stress contours corresponding to $\sigma_e \ge \bar{\sigma}_u$ with increased pressure for shallow and deep flaw pipes with groove and rectangular-shaped defects. The material properties for the analyses covered in these plots correspond to $n = 10$ and $E/\sigma_{ys} = 500$ which are representative of a moderately hardening material such as an API X60 ~ X70 pipeline steel.

The effect of defect shape on the spatial extent of the stress contours is amply demonstrated by comparing the results shown in these plots. For the groove-shaped flaw shown in Figs. 8 and 9, the Mises stress zones begin to develop at the root of the groove (which corresponds to the flaw mid-plane) and then spread across the entire ligament along an angular position of ~45°. It is interesting to note that the angular extension and the forward swing of the plastic lobes resemble to some extent the development of plastic zones for axially cracked pipes subjected to rather strong negative *T*-stress fields (see the extensive analyses and discussion provided by Cravero and Ruggieri [25]). In contrast, a different picture emerges for the growth of stress contours for the rectangular-shaped defects shown in Figs. 10 and 11. Here, the Mises stress zones begin to develop at the corners of the (rectangular) defect after which they coalesce and progress across the entire ligament towards the defect mid-plane. In all analyzed cases, the plastic zones where the Mises stress exceeds the tensile stress, $\bar{\sigma}_u$, spreads rapidly across the ligament with rather little increase in internal pressure. Consider, for example, the deep flaw ($a/t = 0.5$) pipes with groove and rectangular-shaped defects. Development of the Mises stress contours corresponding to $\sigma_e \ge \bar{\sigma}_u$ begins at pressure levels of $\approx 18.2 \sim 18.5$ MPa whereas the fully plastic state of the ligament is reached at pressure levels of $\approx 18.9 \sim 20.7$ MPa.

Although not shown here in interest of space, very similar trends are also displayed for the analyzed pipe configurations with other material properties represented by a hardening exponent of $n = 5$ ($E/\sigma_{ys} = 800$) and $n = 20$ ($E/\sigma_{ys} = 300$). In particular, the low hardening property ($n = 20$) is typical of a high strength steel such as an API X80 ~ X100 pipeline steel. The spatial extent of the Mises stress zones for shallow and deep flaw pipes with groove and rectangular-shaped defects for other material sets develops in much the same way as those shown in previous Figs. 8–11. However, despite the strong similarities in the growth of Mises stress contours for both defect geometries, strain hardening does affect the pressure level at which plastic instability of the remaining ligament occurs. This issue is addressed in more details in the following section.

4.2. Failure pressure for pipes with axial defects

While the previous contour maps for which $\sigma_e \ge \bar{\sigma}_u$ differ significantly for groove and rectangular-shaped defects, the

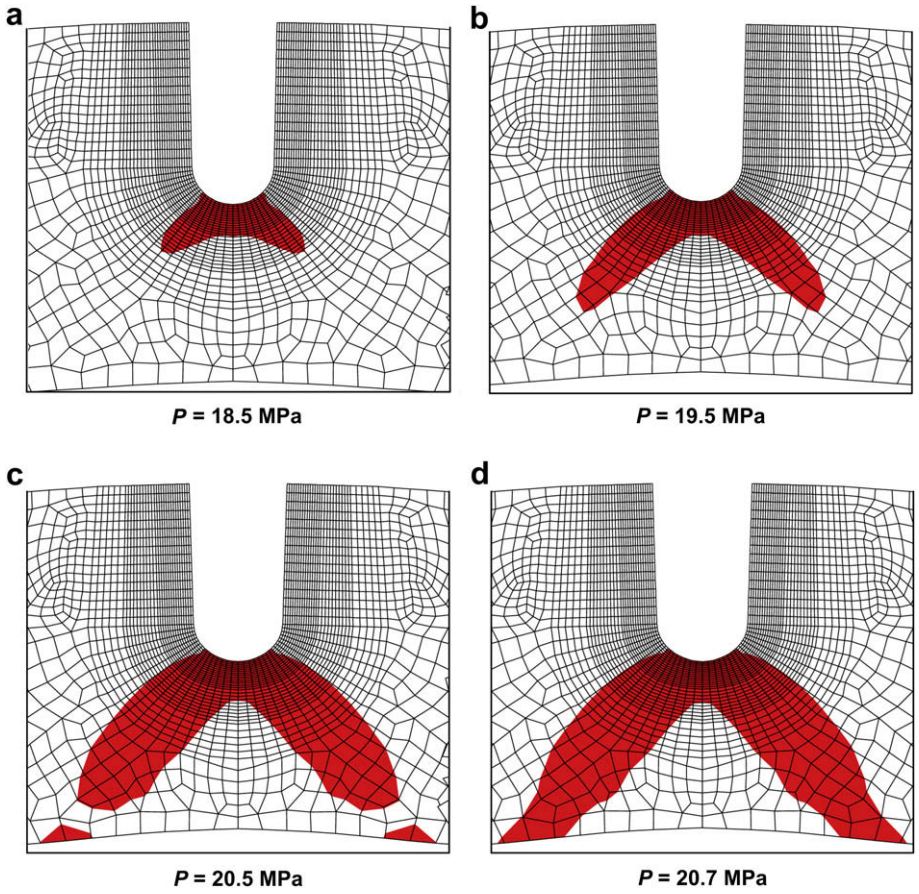

Fig. 8. Mises stress contours with increased internal pressure for the deep flaw ($a/t = 0.5$) pipe with groove-shaped defect and $n = 10$.

previous results clearly provide a connection between plastic instability of the ligament and the attainment of a local limit load. Another key issue to resolve with the applicability of a stress-based criterion in burst pressure predictions of corroded pipelines lies in the effect of the growth and pattern for the evolving stress contours on the local limit load. Here, we examine the influence of defect shape and defect width on the failure pressure for the analyzed pipes.

Figs. 12 and 13 provide the failure pressure, P_f, for shallow and deep flaw pipes with groove and rectangular-shaped defects with

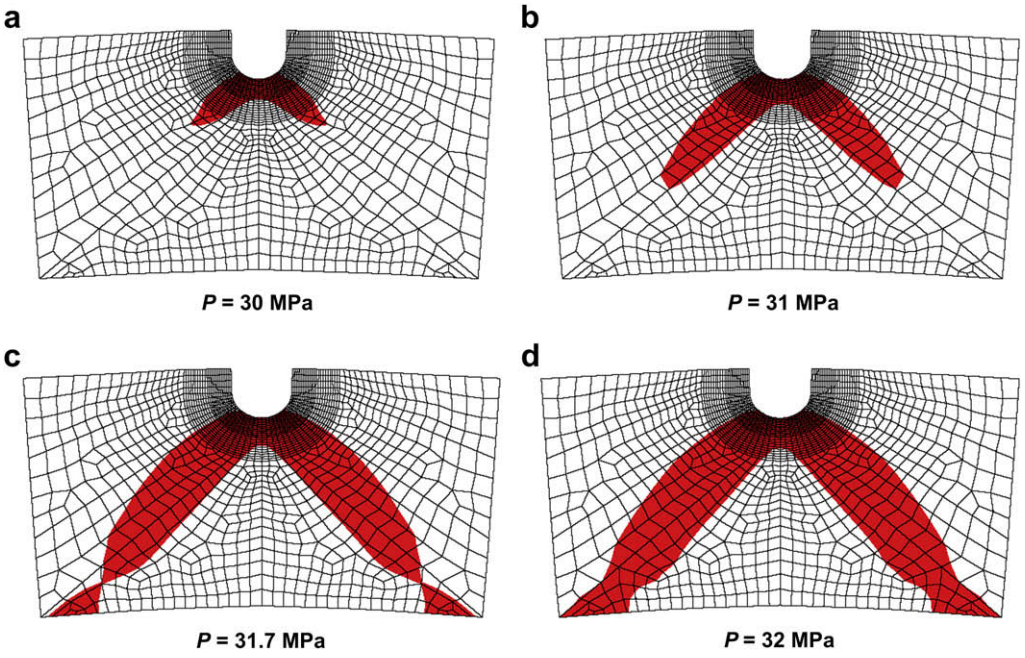

Fig. 9. Mises stress contours with increased internal pressure for the shallow flaw ($a/t = 0.2$) pipe with groove-shaped defect and $n = 10$.

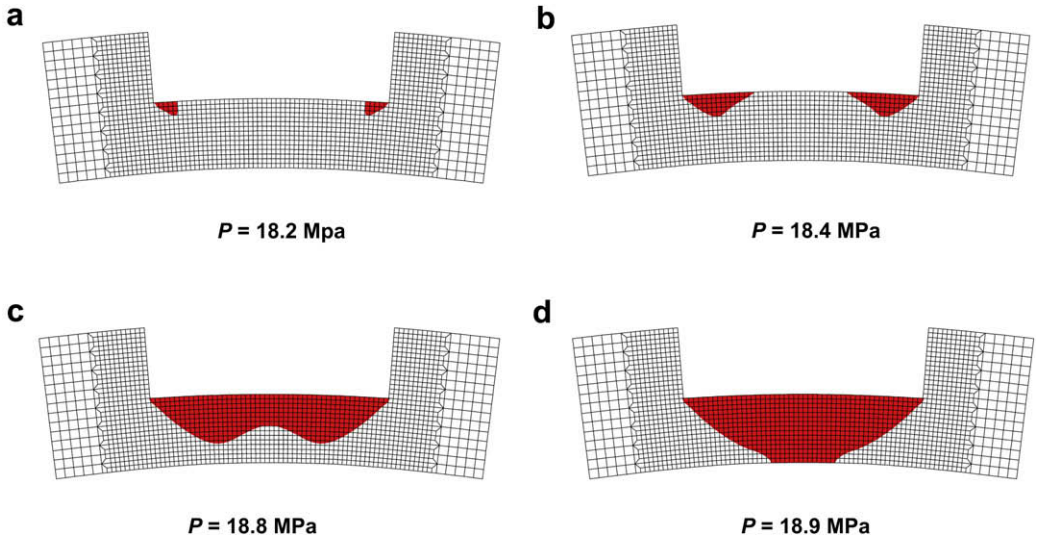

Fig. 10. Mises stress contours with increased internal pressure for the deep flaw ($a/t = 0.5$) pipe with rectangular-shaped defect and $n = 10$.

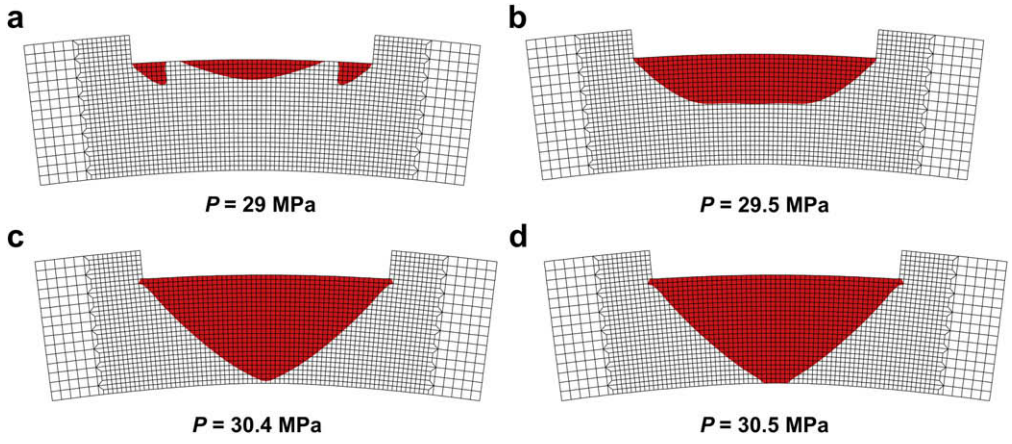

Fig. 11. Mises stress contours with increased internal pressure for the shallow flaw ($a/t = 0.2$) pipe with rectangular-shaped defect and $n = 10$.

varying defect width. Here, the failure pressure is defined by plastic instability of the ligament as shown previously. The material properties correspond to $n = 10$ and $E/\sigma_{ys} = 500$. In the plots, the failure pressure is normalized by the burst pressure solution for a defect-free pipe, P_0, provided by Zhu and Leis [27] in the form

$$P_0 = \left(\frac{C}{2}\right)^{\frac{n+1}{n}} \frac{4t}{D_m} \overline{\sigma}_u \tag{11}$$

where C is a yield-criterion dependent constant, n is the strain hardening exponent, D_m is the average pipe diameter, t is the pipe wall thickness and $\overline{\sigma}_u$ is the material's true tensile strength. In the above expression, the value $C = 2/\sqrt{3}$ as determined by the von Mises yield criterion is adopted in present analyses and provides an upper bound estimate for the failure pressure of a defect-free pipe. To further explore the significance of the adopted failure stress

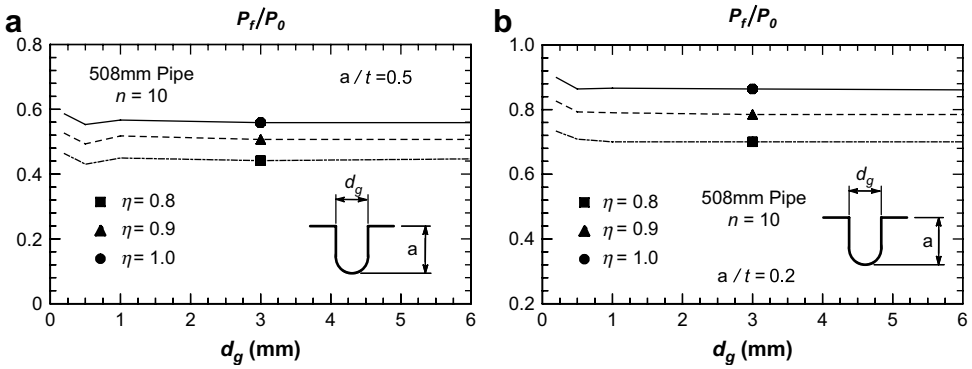

Fig. 12. Dependence of normalized failure pressure on defect width for the $n = 10$ pipe with groove-shaped defect and varying η-parameters. (a) $a/t = 0.5$; (b) $a/t = 0.2$.

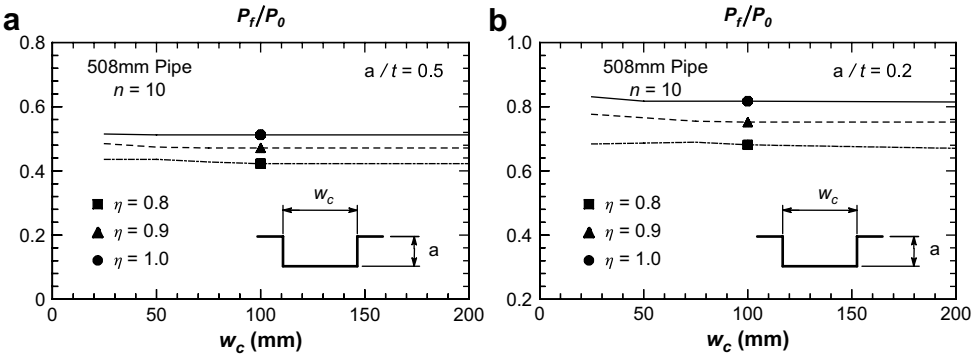

Fig. 13. Dependence of normalized failure pressure on defect width for the $n = 10$ pipe with rectangular-shaped defect and varying η-parameters. (a) $a/t = 0.5$; (b) $a/t = 0.2$.

criterion, the analyses consider plastic instability of the ligament defined by $\sigma_e \geq \eta\overline{\sigma}_u$ where η takes the values 0.8, 0.9 and 1.0.

Not surprisingly, there is a negligible effect of defect width for both defect shapes on the normalized failure pressure for all adopted η-values. The results for the groove-shaped defect displayed in Fig. 12(a, b) reveal a slight elevation in failure pressure for $d_g = 0.2$ mm which is most likely associated with the development of plasticity and strong stress gradients due to the very narrow groove size adopted. Following this short "transient", however, the failure pressure remains essentially constant over the entire range of groove size. The results plotted in Fig. 13 for the rectangular-shaped defect also show virtually no effect of defect width on the normalized pressure. Note, however, a slight decrease in the failure pressure for both deep and shallow flaw when compared with corresponding failure pressures for the groove-shaped defect. The results displayed in Figs. 12 and 13 also show that, for a fixed hardening exponent ($n = 10$ in the analyzed case), the η-factor has a somewhat stronger influence on the failure pressure for the shallow defect. Moreover, the choice of the η-value has no effect on the near invariance of failure pressure with defect size but a rather significant influence on the failure pressure levels. Such behavior can be traced to the evolving Mises stress contours with increased pressure displayed in previous section. The contour maps for which now $\sigma_e \geq \eta\overline{\sigma}_u$ at a fixed pressure level change in extension across the ligament not in shape for different η-values. Consequently, the failure pressure scales almost linearly with increased values of η for the analyzed plane-strain models.

The effect of strain hardening on the normalized failure pressure as defined by attainment of ligament instability at $\sigma_e \geq \overline{\sigma}_u$ is shown in Fig. 14(a,b) for both defect shapes and $a/t = 0.2$ (shallow flaw). The independence of failure pressure on defect width persists for the $n = 5$ and $n = 20$ materials. As already noted in the previous section, this behavior reflects the observation that the general development and spatial extent of the Mises stress contours remain essentially unchanged for varying hardening properties. However, the results in Fig. 14 reveal that the levels of P_f at which $\sigma_e \geq \overline{\sigma}_u$ across the ligament depend on the strain hardening exponent (also recall that P is normalized by P_0 which depends rather strongly on the material's tensile strength, σ_u). Here, the hardening exponent displays a slightly greater impact on the P_f-values for the groove-shaped defects. Overall, however, the adopted failure criterion based upon plastic instability of defect ligament clearly holds true irrespective of the material property. Essentially similar behavior is observed for the deep flaw pipe with $a/t = 0.5$; to conserve space, these results are not shown.

5. Application to burst pressure testing of corroded pipes

5.1. Burst testing of API X65 pipe specimens

Kim et al. [14] performed full scale burst tests on end-capped, pipe specimens with outside diameter, $D = 762$ mm (30 in.), wall thickness, $t = 17.5$ mm, and length, $L = 2.3$ m at room temperature. The material is an API 5L Grade X65 pipeline steel with 495 MPa yield stress and relatively low hardening properties ($\overline{\sigma}_u/\sigma_{ys} = 1.14$). Fig. 7(b) shows the true stress-logarithmic strain curve at test temperature (20 °C) for the material used in the finite element analyses of the pipe specimens.

Testing of the pipe specimens included externally machined corrosion defects positioned on the pipe body and on the pipe welds (seam weld and girth weld). The present work focuses on failure assessments for the tested pipes with corrosion defects machined on the pipe body (see Fig. 5). The corrosion defects have fixed depth, $a = 8.75$ mm, circumferential extent (width), $w_c = 50$ mm and varying corrosion length, $2c = 50$, 100, 200, 300, 600 and 900 mm. Table 1 provides the burst pressures

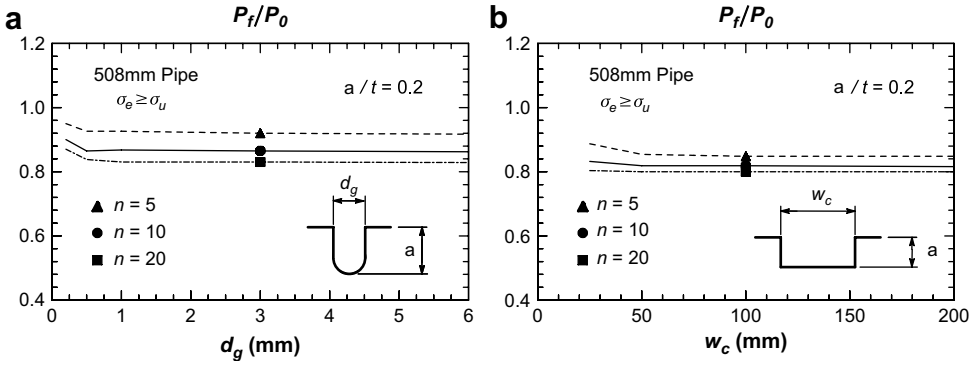

Fig. 14. Dependence of normalized failure pressure on defect width for the shallow flaw pipe ($a/t = 0.2$) with varying hardening properties and $\eta = 1.0$. (a) Grooved-shaped defect; (b) Rectangular-shaped defect.

Table 1
Comparison of measured and predicted burst pressures for the pipe specimens tested by Kim et al. [14] based upon the attainment of plastic instability in defect ligament.

Pipe specimen $2c$ (mm)	$P_{f-\text{exp}}$ (MPa)	$P_{f-\text{pred}}$ (MPa) $\eta=1.0$	$P_{f-\text{pred}}$ (MPa) $\eta=0.9$	$P_{f-\text{pred}}$ (MPa) $\eta=0.85$	$P_{f-\text{pred}}$ (MPa) $\eta=0.8$
50	27.5	25.9	25.8	24.8	20.1
100	24.3	25.7	25.6	21.8	18.1
200	21.8	24.6	23.0	18.8	16.3
300	19.8	22.5	20.1	16.6	15.2
600	16.5	18.5	16.5	15.0	14.4
900	15.0	17.0	15.6	14.9	14.4

experimentally measured in the tests, denoted by $P_{f-\text{exp}}$, with increased corrosion length, $2c$.

Failure assessments for the tested pipe specimens with external corrosion defects follow the limit load analysis based upon the evolution of Mises stress contours across the defect ligament outlined in Section 4. Fig. 15 compares burst pressure predictions, hereafter denoted as $P_{f-\text{pred}}$, derived from the attainment of ligament instability defined in terms of $\sigma_e \geq \eta\overline{\sigma}_u$, where η takes the values 0.8, 0.85, 0.9 and 1.0, for the 3-D models described in Section 3.2. The solid symbols in the plots represent the corresponding predicted values while the solid line defines equality between the experiments and predictions, i.e., $P_{f-\text{exp}} = P_{f-\text{pred}}$. The plot also includes the predicted pressure values for the pipes using the ASME B31.G [2] and DNV RP-F101 [4] procedures; here, the open symbols represent the predicted values. Table 1 compares the predicted burst pressures for different η-values with the experimentally measured values for increased defect length, $2c$. To facilitate interpretation of the effect of defect length on predicted failure pressures, the arrow shown in Fig. 15 indicates increased failure pressure with decreased defect length.

These results clearly reveal the strong effect of the η-values on predicted failure pressures based upon ligament instability. For $\eta = 1.0$, the analyses consistently overpredict the failure pressure for almost the entire range of defect length by as much as 15%; here, only the predicted failure pressure for the pipe specimen with very short defect, $2c = 50$ mm, is below the measured failure pressure. By contrast, all the analyses with $\eta = 0.8$ underpredict the failure pressure for all defect lengths with rather significant deviations from the measured values for short defects ($2c \leq 200 \sim 300$ mm). Predictions derived from using $\eta = 0.9$ display better agreement with experimental data but the analyses also overestimate the

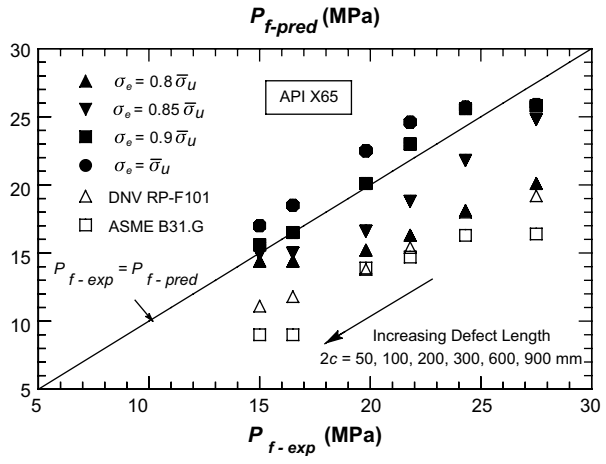

Fig. 15. Comparison between predicted and experimental burst pressures for the X65 pipe specimens tested by Kim et al. [14].

Table 2
Comparison of measured and predicted burst pressures for the pipe specimens tested by Mannucci et al. [15] based upon the attainment of plastic instability in defect ligament.

Pipe specimen $D/2c \times a$ (mm)	$P_{f-\text{exp}}$ (MPa)	$P_{f-\text{pred}}$ (MPa) $\eta=1.0$	$P_{f-\text{pred}}$ (MPa) $\eta=0.9$	$P_{f-\text{pred}}$ (MPa) $\eta=0.85$	$P_{f-\text{pred}}$ (MPa) $\eta=0.8$
$1422/180 \times 10.4$	15.4	18.4	12.9	12.2	11.8
$914/150 \times 9$	21.4	25.7	19.1	17.1	16.1
$914/450 \times 6$	24.0	26.1	22.3	20.1	19.6

measured failure pressure for the pipe specimens by a factor of ≈5%; again, only the failure pressure for the shortest defect length ($2c = 50$ mm) is slightly underestimated. For this analyzed data set, adoption of an η-value in the range of ≈0.85 reduces the excessive pessimism in failure pressure predictions which arises from the use of too low values for η while, at the same time, providing more adequate safety margins. Moreover, consistent with previous studies, prediction analyses based upon the ASME B31.G and DNV RP-F101 procedures yield large margins between experimental values and predicted results for all pipe specimens, particularly in the case of the ASME methodology.

5.2. Burst testing of API X100 pipe specimens

Additional analyses conducted on very thin-walled, large diameter pipes made of low hardening, high strength steel enable further verification studies of the ligament instability methodology described in the present work. Here we describe the results of detailed 3-D analyses to predict the burst pressure for the pipe specimens tested by Mannucci et al. [15]. The pipe and defect geometries were previously introduced in Section 3. The material is an API 5L Grade X100 pipeline steel with 740 ~ 795 MPa yield stress and very low hardening properties ($\sigma_u/\sigma_{ys} = 1.04 \sim 1.09$) – see Ref. [15] for details. Table 2 provides the experimentally measured burst pressure for each tested pipe specimen.

Failure assessments for the pipe specimens with axial surface defects again follow the limit load analysis outlined in Section 4 based upon the attainment of ligament instability defined in terms of $\sigma_e \geq \eta\overline{\sigma}_u$, where η takes the values 0.8, 0.85, 0.9 and 1.0. Fig. 16 provides the predicted burst pressures, $P_{f-\text{pred}}$, for the 3-D models described in Section 3.3. The solid symbols in the plots represent the predicted values while the solid line defines equality between the experiments and predictions. The open symbols in the plot

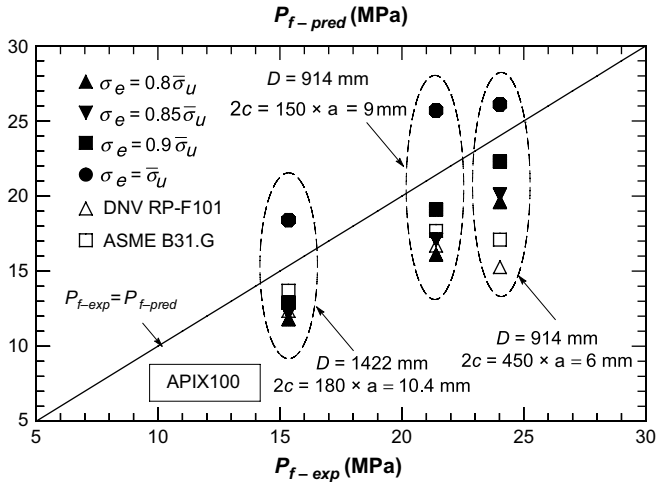

Fig. 16. Comparison between predicted and experimental burst pressures for the X100 pipe specimens tested by Mannucci et al. [15].

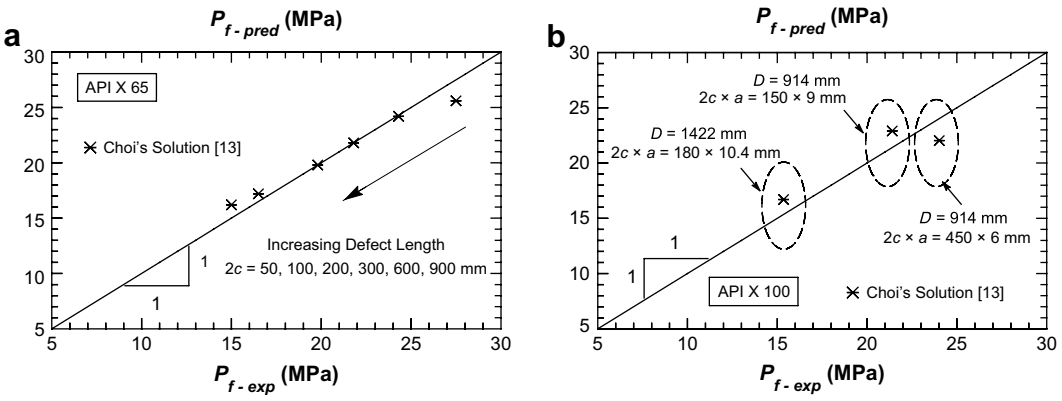

Fig. 17. Comparison between the limit load solution given by Choi et al. [13] and experimental burst pressures. (a) X65 pipe specimens; (b) X100 pipe specimens.

represent the predicted values derived from using the ASME B31.G [2] and DNV RP-F101 [4] procedures. Table 2 compares the predicted burst pressures for different η-values with the experimentally measured values for each tested pipe.

In contrast to the instability analysis for the X65 pipes, the predicted burst pressures for the X100 pipes exhibit a somewhat weaker dependence on the η-value. Apart from the predictions based upon $\eta = 1.0$ in which all failure pressure values lie above the 1:1 line, the predicted burst pressures for all analyzed pipe specimens agree relatively well with experimental data, particularly for $\eta = 0.9$. Further, prediction analyses based upon the ASME B31.G and DNV RP-F101 procedures reveal a mixed behavior. For the pipe specimens with $D = 914$ mm (36 in.), these procedures yield large margins between experimental values and predicted results, particularly for the defect with $2c = 450 \times a = 6$ mm. However, for the pipe specimens with $D = 1422$ mm (56 in.), both the ASME and DNV procedures provide a better agreement with the measured failure pressure.

5.3. Comparison with limit load solutions for corrosion defect assessments

The limit load procedure to predict the burst pressure in flawed pipes discussed thus far relies explicitly on detailed, nonlinear finite element analysis to determine plastic instability of the remaining ligament. Here, we compare the experimentally measured failure pressure for the previous tested pipes with predictions based upon a recent limit load solution for corrosion defect assessments proposed by Choi et al. [13]. While other alternative solutions are available (see, *e.g.*, [22–24]), we favor Choi's solution because of its relative simplicity and rather extensive calibration derived from numerical analyses conducted on models for thin-walled corroded pipes with varying D/t-ratio and defect geometry.

Fig. 17(a, b) shows the predicted burst pressures for the tested pipe specimens (X65 and X100 materials) based upon Choi's limit load solution. A solid line defining equality between the experiments and predictions is also provided to facilitate interpretation of the results. Consider first the X65 data set. General good agreement is observed between predictions and experiments; for this data set, the adopted limit load solution slightly overpredicts the failure pressures for long corrosion defects ($2c = 600$ and 900 mm). Consider now the X100 data set. Apart from the pipe specimen with $D = 914$ mm (36 in.) and $2c = 450 \times a = 6$ mm, the predicted failure pressures overestimate the measured values by a factor of $\sim$10%. Because the limit load solution provided by Choi et al. [13] is also based upon the criterion $\sigma_e \geq \eta\overline{\sigma}_u$ with $\eta = 0.9$, these analyses, albeit rather limited, further indicate the potential dependence of a "correct" choice for the η-value upon defect geometry and hardening behavior.

6. Discussion and concluding remarks

The parametric analyses of local ligament instability for flawed pipes described here, coupled with verification studies to predict experimentally measured burst pressure, provide an additional support to use stress-based criteria in defect assessments of corroded pipelines. The analyses consider a failure criterion based upon the evolution of the highly stressed zones in the remaining defect ligament until the attainment of a local limit load. Within the methodology pursued in the present work, such criterion translates into a simple description of ligament instability defined by $\sigma_e \geq \eta\overline{\sigma}_u$ where $\overline{\sigma}_u$ is the true ultimate tensile strength and η often ranges from 0.8 to 1.0.

Since the core of such an approach is the adoption of a stress reduction factor applied to the materials tensile strength, it is natural to raise the question as which η-value suffices to adequately describe ligament instability leading to pipe failure. While the use of $\eta = 1.0$ in the present context preserves the widely adopted plastic instability criterion for geometries subjected to predominantly tensile loading, it does not appear to fully describe the actual mechanical behavior of pressurized pipes with axial defects. Indeed, for a thin-walled pipe with an external axial flaw under increased pressure, the outward deflection (for an external defect) caused by the bulging of the pipe often complicates the stress distribution in the defect ligament due to the impingement of a bend field on the hoop stress distribution (see illustrative example in Ref. [32]). Moreover, the failure stress criterion implies the adoption of a yield theory to define the equivalent stress acting on the ligament which may also potentially affect the predicted burst pressure. This argument can be understood by considering that the Tresca criterion generally predicts lower bound failure pressures whereas the von Mises criterion provides upper bound failure pressures [27]. The stress reduction factor given by the η parameter associated with the failure criterion thus provides a certain degree of trade-off between some inherent uncertainties present in the model and the actual pipe behavior.

Extensive plane-strain analyses conducted on pipe models with axial flaws demonstrate the independence of the ligament instability criterion on key geometrical and material parameters controlling the failure pressure, including defect shape (groove *vs.* rectangle), and defect width. A central result derived from these analyses is that burst pressure defined by attainment of plastic instability of defect ligament displays very weak sensitivity on defect shape even though the contour maps for which $\sigma_e \geq \overline{\sigma}_u$ differ significantly for groove and rectangular-shaped defects. This conclusion suggests that the computational demands to accurately model the correct defect shape can be minimized while maintaining an adequate resolution of ligament stresses.

Verification analyses using experimentally measured burst pressure data for corroded pipe specimens made of API X65 and

X100 pipeline steel further indicate the capability of the stress-based criterion defined in terms of ligament instability to predict the failure pressure for the tested pipes. While rather limited, the analysis results demonstrate the overall effectiveness of the proposed stress-based criterion using $\sigma_{\text{ref}} \geq \eta\overline{\sigma}_{\text{u}}$ in burst pressure predictions. However, for the experimental data sets (API X65 and X100 pipe specimens) considered here, the η-factor appears to exhibit a potential dependence on defect geometry and material's strain hardening capacity. This feature can adversely affect predictions and potentially hinder the "correct" safety margin as there is a mixed trend in degree of conservatism/pessimism for the present analyses. Further verification studies based upon a recently proposed limit load solution [13] most applicable to thin-walled corroded pipelines also confirm these observed trends. Such conclusions may also raise some concern about the applicability of current limit load solutions for axially cracked and corroded pipes embodied into current defect assessment procedures such as, for example, API 579 [20] and SINTAP [19]. Although additional experimental and numerical studies appear necessary to establish a more general range of η-factors applicable to thin-walled pipes with varying geometry (including defect configuration) and material properties, the results presented here provide a compelling support to use stress-based approaches incorporating ligament instability analyses in defect assessments of corroded pipelines.

Acknowledgements

This investigation is supported by the Brazilian Council for Scientific and Technological Development (CNPq). The valuable comments by a reviewer are gratefully acknowledged.

References

[1] Eiber RJ, Kiefner JF. Failure of pipelines. In: Failure analysis and prevention. Metals handbook. 9th ed., vol. 11. American Society for Metals; 1986. p. 695–706.
[2] American Society of Mechanical Engineers. Manual for determining the remaining strength of corroded pipelines. B31G. Three Park Avenue, New York: ASME; 1991.
[3] Kiefner JF, Vieth PH. A modified criterion for evaluating the remaining strength of corroded pipe. Final report on project PR 3-805. Batelle, Ohio: Pipeline Research Committee, American Gas Association; 1989.
[4] Det Norsk Veritas. Corroded Pipelines, DNV-RP-F101; 2004.
[5] Kiefner JF, Maxey WA, Eiber RJ, Duffy AR. Failure stress levels of flaws in pressurized cylinders. ASTM STP 536. In: Progress in flaw growth and fracture toughness testing. Philadelphia: American Society for Testing and Materials; 1973. p. 461–81.
[6] Batte A D, Fu B, Kirkwood MG,Vu D. New methods for determining the remaining strength of corroded pipelines in offshore mechanics and arctic engineering conference (OMAE), vol. V; 1997. p. 221–8 [Pipeline Technology].
[7] Leis BN, Stephens DR. An alternative approach to assess the integrity of corroded line pipe – Part I: current status In: International offshore and polar engineering conference (ISOPE), vol. IV; 1997. p. 624–34.
[8] Wilkowski G, Stephens G, Krishnaswamy P, Leis B, Rudland D. "Progress in development of acceptance criteria for local thinned areas in pipe and piping components. Nuclear Engineering and Design 2000;195:149–69.
[9] Maes MA, Salama MM, Dann M. Reliability of burst limit states for damaged and corroded high strength pipelines. In: twenty-fifth offshore mechanics and arctic engineering conference (OMAE); 2006.
[10] Fu B, Kirkwood M.G. Determination of Failure pressure of corroded linepipes using the nonlinear finite element method. In: Proceedings of the second International pipeline technology conference, vol. II; 1995. p. 1–9.
[11] Karstensen A, Smith A, Smith S. Corrosion damage assessment and burst test validation of 8in X52 linepipe. Pressure Vessel Piping Design Analysis 2001;430:189–94.
[12] Noronha D B, Benjamin AC, Andrade EQ. Finite element models for the prediction of the failure pressure of pipelines with long corrosion defects. In international pipeline conference (IPC). Calgary, Alberta, Canada; 2002.
[13] Choi JB, Goo BK, Kim JC, Kim YJ, Kim WS. Development of limit load solutions for corroded gas pipelines. International Journal of Pressure Vessels and Piping 2003;80:121–8.
[14] Kim YP, Kim WS, Lee YK, Oh KH. The evaluation of failure pressure for corrosion defects within girth or seam weld in transmission pipelines. In: international pipeline conference (IPC). Calgary, Alberta, Canada; 2004.
[15] Mannucci G, Demofonti G, Barsanti L, Harris D,Hillenbrand HG. Fracture properties of API X100 gas pipeline steels. In: Thirteenth Biennial EPRG-PRCI Joint technical meeting. New Orleans, Louisiana, USA; 2001.
[16] Chakrabarty J. Theory of plasticity. 3rd ed. Oxford: Elsevier B.V.; 2006.
[17] Miller AG. Review of limit loads of structures containing defects. International Journal of Pressure Vessels and Piping 1988;32:197–327.
[18] British Standard Institution. Guide on methods for assessing the acceptability of flaws in metallic structures. BS7910; 1999.
[19] SINTAP: Structural Integrity Assessment Procedure for European Industry. Final procedure; 1999.
[20] American Petroleum Institute. Fitness-for-service. API RP-579-1/ASME FFS-1, 2007.
[21] Carter. J. A library of limit loads for fracture.Two. Nuclear electric report TD/SID/REP/0191; 1991.
[22] Staat M. Plastic collapse analysis of longitudinally flawed pipes and vessels. Nuclear Engineering and Design 2004;234:25–43.
[23] Staat M. Local and global collapse pressure of longitudinally flawed pipes and cylindrical vessels. International Journal of Pressure Vessels and Piping 2005;82:217–25.
[24] Staat M, Vu DK. Limit analysis of flaws in pressurized pipes and cylindrical vessels. Part I: axial defects. Engineering Fracture Mechanics 2007;74:431–50.
[25] Cravero S, Ruggieri C. Correlation of fracture behavior in high pressure pipelines with axial flaws using constraint designed test specimens – Part I: plane-strain analyses. Engineering Fracture Mechanics 2005;72:1344–60.
[26] Silva LAL, Cravero S, Ruggieri C. Correlation of fracture behavior in high pressure pipelines with axial flaws using constraint designed test specimens – Part II: 3-D effects on constraint. Engineering Fracture Mechanics 2006;73:2123–38.
[27] Zhu XK, Leis BN. Theoretical and numerical predictions of burst pressure of pipelines. In: ASME pressure vessels and piping division conference (PVP). Vancouver, BC, Canada; 2005.
[28] Anderson TL. Fracture mechanics: fundaments and applications. 3rd ed. New York: CRC Press; 2005.
[29] Folias ES. The stresses in a cylindrical shell containing an axial crack", aerospace research laboratories. Report ARL, 1964. p. 64–174.
[30] Folias ES. An axial crack in a pressurized cylindrical shell. International Journal of Fracture Mechanics 1965;1:104–13.
[31] Koppenhoefer K, Gullerud A, Ruggieri C, Dodds R, Healy B. WARP3D: dynamic nonlinear analysis of solids using a preconditioned conjugate gradient software architecture. UILU-ENG-94-2017. In: Structural Research Series (SRS) 596. University of Illinois at Urbana–Champaign; 1994.
[32] Dotta F, Ruggieri C. "Structural integrity assessments of high pressure pipelines with axial flaws using a micromechanics model. International Journal of Pressure Vessels and Piping 2004;81:761–70.